Circulation

ORIGINAL RESEARCH ARTICLE

Early Cardiac Remodeling Promotes Tumor Growth and Metastasis

Editorial, see p 684

BACKGROUND: Recent evidence suggests that cancer and cardiovascular diseases are associated. Chemotherapy drugs are known to result in cardiotoxicity, and studies have shown that heart failure and stress correlate with poor cancer prognosis. However, whether cardiac remodeling in the absence of heart failure is sufficient to promote cancer is unknown.

METHODS: To investigate the effect of early cardiac remodeling on tumor growth and metastasis colonization, we used transverse aortic constriction (TAC), a model for pressure overload–induced cardiac hypertrophy, and followed it by cancer cell implantation.

RESULTS: TAC-operated mice developed larger primary tumors with a higher proliferation rate and displayed more metastatic lesions compared with controls. Serum derived from TAC-operated mice potentiated cancer cell proliferation in vitro, suggesting the existence of secreted tumor-promoting factors. Using RNA-sequencing data, we identified elevated mRNA levels of periostin in the hearts of TAC-operated mice. Periostin levels were also found to be high in the serum after TAC. Depletion of periostin from the serum abrogated the proliferation of cancer cells; conversely, the addition of periostin enhanced cancer cell proliferation in vitro. This is the first study to show that early cardiac remodeling nurtures tumor growth and metastasis and therefore promotes cancer progression.

CONCLUSIONS: Our study highlights the importance of early diagnosis and treatment of cardiac remodeling because it may attenuate cancer progression and improve cancer outcome.

Shimrit Avraham, PhD
Soraya Abu-Sharki, BSc
Rona Shofti, DVM, PhD
Tali Haas, DVM
Ben Korin, PhD
Roy Kalfon, PhD
Tom Friedman, MD
Avinoam Shiran, MD
Walid Saliba, MD, MPH
Yuval Shaked, PhD
Ami Aronheim, PhD

Key Words: aortic stenosis ■ constriction ■ neoplasm metastasis ■ neoplasms ■ periostin-like factor, mouse ■ ventricular remodeling

Sources of Funding, see page 682

https://www.ahajournals.org/journal/circ

Clinical Perspective

What Is New?

- Heart failure correlates with poor cancer prognosis, yet it remains unclear whether cardiac remodeling in the absence of heart failure is sufficient to promote cancer progression.
- This is the first study to show that early cardiac remodeling promotes tumor growth and metastasis, possibly via secreted factors.
- Periostin was identified as an extracellular matrix protein secreted from the remodeled heart and associated with cancer progression as a putative mediator of this effect.

What Are the Clinical Implications?

- We speculate that it may be recommended to consider cancer surveillance at early stages of cardiac remodeling among patients with preexisting risk factors for cancer.
- Cardiac secreted factors that potentially promote cancer growth can serve as predictors of poor outcome in patients with cancer and may be incorporated in future risk stratifications models.
- Further study is needed to test the hypothesis that early aortic valve replacement may reduce cancer risk.

Pathological hypertrophic growth of cardiac muscle is an adaptive response to mechanophysical, metabolic, or genetic stress.[1] Sustained and chronic cardiac stress turns the adaptive response into a maladaptive process, leading to contractile dysfunction and heart failure (HF).[2] Cardiac hypertrophy is linked to clinically relevant diseases such as hypertension, myocardial infarction, coronary artery disease, valvular disease, and obesity-induced cardiomyopathy.[3–5] Advances in the treatment for cardiovascular risk factors reduced HF outcome and increased life span.[6] The latter results in cardiovascular patients exposure to aging diseases such as cancer.[7]

Cardiac growth was considered a tumor-like growth. The biological principles of cell growth, death, and survival are as important in the onset of HF as in tumor progression.[8] In addition, cell proliferation molecular signals and cardiac myocyte hypertrophy are highly conserved.[9] Cardiac diseases and cancer share similar risk factors: genetic predisposition, smoking, obesity, hyperlipidemia, sedentary lifestyle, diabetes mellitus, and aging.[7,10] Although HF and cancer were considered separate diseases, it appears that they are highly connected and affect each other's outcome at multiple levels.[10,11] Multiple epidemiological studies suggest that patients with HF are at higher risk to develop cancer with poorer outcomes.[10–13]

The communication between both heart and tumor with all other organs in the body occurs through secreted factors, which regulate the fate of both diseases.[14,15] A recent study has shown that HF after myocardial infarction in mice with spontaneous intestinal adenoma formation resulted in enhanced tumor load.[16] However, although some evidence connecting HF and cancer exists, it is unknown whether early cardiac remodeling in the absence of HF is sufficient to promote cancer severity and outcome.

Here, we studied whether the early stages of cardiac remodeling promote cancer progression and spread. To depict early cardiac remodeling, we used transverse aortic constriction (TAC), an experimental model for pressure overload–induced cardiac hypertrophy, which also occurs in aortic stenosis (AS) in patients. Subsequently, we implanted mice with 2 cancer models, an orthotopic breast cancer model (polyoma middle T [PyMT] cells) and a syngeneic lung cancer model (Lewis lung carcinoma [LLC]). We show that TAC-operated mice developed larger primary tumors and displayed higher metastatic seeding rate compared with control mice, indicating that TAC promotes cancer progression. Moreover, by analyzing an echocardiography database, we show that patients with moderate to severe AS are prone to develop nonhematologic cancer compared with patients without AS. Furthermore, AS emerges as a possible risk factor for cancer in 40- to 60-year-old patients.

These results highlight the importance of early diagnosis and treatment of cardiac remodeling because it may balance the potential causal effects of cardiac disease on cancer progression.

METHODS

The authors declare that all supporting data are available within the article and its online supplementary files except for the human data. Because of the sensitive nature of the data collected for this study, requests to access the data set from qualified researchers trained in human subject confidentiality protocols may be sent to Dr Saliba at the Department of Community Medicine and Epidemiology, Lady Davis Carmel Medical Center (saliba_wa@clalit.org.il).

Animals

Age-matched C57Bl/6, NOD/SCID (nonobese diabetic/severe combined immunodeficiency), and maladaptive cardiac remodeling–resistant (MCRR) female and male mice (8–10 weeks old) were used. MCRR mice are genetically modified, harboring inactivation mutations in JDP2 (c-Jun dimerization protein 2) and activating transcription factor 3.[17] Mice were bred and raised at the Pre-Clinical Research Authority at the Ruth and Bruce Rappaport Faculty of Medicine. Experiments were performed following Institutional Animal Care and Use Committee approval and according to the Israeli welfare act, which abides by the National Research Council guidelines, and according to the *Guide for the Care and Use of Laboratory Animals* of the National Institute of Health (IL-003-01-19). Procedures were carried out under isoflurane anesthesia.

TAC Surgery

TAC surgery was performed on male and female mice (8–10 weeks old) as previously described.[18] Constriction was applied with a 27-gauge blunt needle to create a standardized constriction of the aorta.

Echocardiography

Mice were anesthetized with 1% isoflurane and kept on a 37°C heated plate throughout the procedure. Echocardiography was performed with a Vevo2100 microultrasound imaging system (VisualSonics, Fujifilm) equipped with 13- to 38-MHz (MS 400) and 22- to 55-MHz (MS550D) linear array transducers. Cardiac size, shape, and function were analyzed by conventional 2-dimensional imaging and M-mode recordings. Maximal left ventricular end-diastolic (LVDd) and end-systolic (LVDs) dimensions were measured in short-axis M-mode images. Fractional shortening (FS) was calculated as follows: FS (percent)=[(LVDd–LVDs)/LVDd]×100. All values were based on the average of at least 3 measurements for each mouse.

Cell Culture

The LLC cell line was purchased from the American Type Culture Collection (ATCC). The PyMT murine breast carcinoma cell line was derived from primary tumor-bearing transgenic mice expressing PyMT under the control of the murine mammary tumor virus promoter[19] (kindly provided by Dr Tsonwin Hai, The Ohio State University). Cell lines were tested and found to be free of mycoplasma contamination. Cells were cultured in DMEM supplemented with 10% (vol/vol) FBS, 1% streptomycin and penicillin, 1% L-glutamine, and 1% sodium (full medium) pyruvate at 37°C in a humidified atmosphere containing 5% CO_2.

Primary Tumor and Metastasis Models

LLC and PyMT cancer cells (5×10^5 or 10^5, respectively) were implanted subcutaneously into the flanks and orthotopically injected into the back left side mammary fat pad, respectively, as previously described.[20] Tumor volume was measured with a caliper, and the tumor volume was calculated with the following formula: $Width^2\times Length\times0.5$. According to the Institutional Animal Care and Use Committee, the humane end point is defined when the average tumor size reaches 1700 mm^3. An experimental pulmonary metastasis assay was carried out with LLC or PyMT cancer cells (2×10^6 or 2×10^5 cells, respectively, in 200 µL PBS) injected into the tail vein, as previously described.[21] At the end point, mice were euthanized, and their hearts, lungs, and tumors were excised and weighed.

Blood Serum

Blood was obtained from the facial vein with a 4-µm sterile Goldenrod Animal Lancet (MEDIpoint, Inc, Mineola, NY). Blood was collected and allowed to clot at room temperature for 2 hours, followed by 15 minutes of centrifugation at 2000*g*. Serum was immediately aliquoted and stored at –20°C for future use.

Cell Proliferation Assay

PyMT or LLC cells were seeded in full medium at a concentration of 5×10^3 cells/mL for 6 hours. After the cells were attached to the plate, the medium was replaced with serum-free medium overnight. Then, the medium was replaced with fresh medium containing 10% (FBS; positive control), serum free (negative control), or 10% mouse serum derived from naive, control, sham, or TAC-operated mice with or without cancer or 1000, 2000, or 4000 ng/mL recombinant mouse periostin (R&D Systems, 2955-F2-050) in 1% FBS DMEM medium. PyMT and LLC cells were left with mouse blood serum or periostin for 24 and 48 hours. Proliferation rate was measured with the CellTiter-Glo Luminescent Cell Viability Assay according to the manufacturer's instructions. Luciferase activity was measured with a TD 20/20 luminometer (Turner Designs, Sunnyvale, CA).

Immunodepletion Assay

Protein G PLUS-Agarose beads (sc-2002, Santa Cruz Biotechnology) were preincubated with an anti-mPeriostin/OSF-2 antibody (R&D Systems, AF2955) or PBS. Then, the beads were blocked with anti-HA tag antibody (12CA5). Beads were incubated with serum derived from sham or TAC-operated mice. *Periostin* depletion was detected by ELISA (Figure I in the Data Supplement). Depleted serum was used to examine cell proliferation of cancer cells as described earlier.

ELISA Test

Quantification of periostin and connective tissue growth factor (CTgF) protein levels in the serum was performed with the Mouse Periostin/OSF-2 Quantikine ELISA Kit (R&D Systems Inc, Minneapolis, MN) and Mouse CTGF-Connective Tissue Growth Factor ELISA Kit (E-EL-M0340, Elabscience, Houston, TX) according to the manufacturer's instructions.

RNA Extraction and Quantitative Polymerase Chain Reaction

Total RNA was extracted from hearts with an Aurum total RNA fatty or fibrous tissue kit (No. 732–6830, Bio-Rad, Hercules, CA) according to the manufacturer's instructions. Next, cDNA was synthesized from 1000 ng purified mRNA with the iScript cDNA Synthesis Kit (No. 170–8891, Bio-Rad). Real-time polymerase chain reaction was performed with Rotor-Gene 6000 (Bosch Institute, Sydney, Australia) with absolute blue SYBER green ROX mix (Thermo Scientific AB-4162/B). Serial dilutions of a standard sample were included for each gene to generate a standard curve. Values were normalized to GAPDH expression levels. The following primers were used: ANP (atrial natriuretic peptide) forward (F), GCTTCCAGGCCATATTGGAG; ANP reverse (R), GGGGGCATGACCTCATCTT; BNP (brain natriuretic peptide)-F, GAGGTCACTCCTATCCTCTGG; BNP-R, GCCATTTCCTCCGACTTTTCTC; β-myosin heavy chain (βMHC)-F, TGCAAAGGCTCCAGGTCTGA; βMHC-R, CTTGA ACCTGTCCAACCACAA; ACTA1-F, GTGAGATTGTGCGCGA CATC; ACTA1-R, GGCAACGGAAACGCTCATT; CTgF-F, AGA CCTGTGGGATGGGCAT; CTgF-R, GCTTGGCGATTTTAG GTGTCC; periostin-F, CCTGCCCTTATATGCTCTGCT; and periostin-R, AAACATGGTCAATAGGCATCACT.

Hematoxylin and Eosin Staining

Lungs were fixed in 4% formaldehyde overnight, embedded in paraffin, subsequently serially sectioned at 6-µm intervals, and then mounted on slides. Hematoxylin and eosin staining was performed according to the standard protocol. Images were acquired with 3DHistech Pannoramic 250 Flash III (3DHISTECH Ltd, Budapest, Hungary). Each section was fully scanned. The area of metastatic lesions was calculated with CaseViewer software.

Immunofluorescence Staining

Tumors were fixed in 4% formaldehyde overnight, embedded in optimal cutting temperature compound, and serially sectioned at 10-µm intervals. Frozen tumor sections were stained for CD31 (BD Biosciences, 553370) and Ki67 (Abcam, ab16667) and counterstained with DAPI, as previously described.[20] Images were acquired with 3DHistech Pannoramic 250 Flash III (3DHISTECH Ltd, Budapest, Hungary). Each section was fully scanned; for each analysis, 5 fields were randomly chosen and blindly and automatically analyzed with ImageJ software.[22] For every dot plot of image analysis, each dot represents the mean of the values taken from 5 fields, derived from a single mouse.

RNA Sequencing Analysis

Quality control for total RNA was performed with TapeStation (Agilent). The RNA integrity number equivalent value of all samples was >7.8. Eight RNA-sequencing (RNA-seq) libraries (NEBNext Ultra RNA Library Prep Kit for Illumina, catalog no. E7530) were produced according to the manufacturer's protocol with 800 ng total RNA. mRNA pull-up was performed with Magnetic Isolation Module (NEB, catalog no. E7490). All 8 libraries were mixed into a single tube with equal molarity. The RNA-seq data were generated on Illumina NextSeq500, 75-bp single-end reads, high-output mode (Illumina, FC-404-2005). Quality control was assessed with Fastqc (version 0.11.5); reads were trimmed for adapters, low quality 3′, and minimum length of 20 with CUTADAPT (version 1.1); 75-bp single-end reads were aligned to mouse reference genome (Mus_musculus.GRCm38.90downloaded from ENSEMBL) with STARaligner (STAR_2.5.3a). The number of reads per gene was counted with Htseq (0.6.0). Statistical analysis was performed with DESeq2 R package (version 1.16.1; Genome Biology 2014 15:550). Similarity between samples was evaluated within the DESeq2 package. The multiple testing correction was Benjamini-Hochberg false discovery rate. Statistical threshold for differential expression was $P_{adjusted}<0.05$ (Table I in the Excel File in the Data Supplement). Gene ontology and pathway enrichment analyses were performed with the WEB-based GEneSeT Analysis Toolkit (WebGestalt) and MetaCore software.[23] Genes encoding for secreted proteins were found by use of the UniProt subcellular location.[24]

Human Data

To assess the association between AS and cancer risk, we used the echocardiography database from Lady Davis Carmel Medical Center, which includes data from both inpatients and outpatients from the Clalit Health Services group in the district of Haifa and Western Galilee. The study was approved by the Review Board of the Lady Davis Carmel Medical Center and conducted in accordance with the Declaration of Helsinki protocol No. 0134-19 CMC. Eligible patients were adults ≥40 years of age who underwent echocardiography between January 1, 2005, and December 31, 2018. Patients who underwent coronary artery bypass surgery or aortic or mitral valve replacement were excluded. Population selection for the study is depicted in Figure II in the Data Supplement. The first dated test of patients with moderate or severe AS (defined as aortic valve area ≤1.5 cm^2) was used to define the exposure group (moderate to severe AS; Figure II in the Data Supplement). The first dated test of patients without evidence of any degree of AS (defined as aortic valve area >2 cm^2 or maximal aortic velocity <2.5 m/s) was used to define the comparative group (no AS).

Statistics

Mouse Studies

Data are presented as mean±SE. All mice were included in each statistical analysis unless they were euthanized for humane reasons before the experimental end point. Experimental groups were blinded to the experimentalists during data collection. Animals were selected for each group in a randomized fashion. Statistical significance of tumor volume was determined by 2-way repeated-measures ANOVA followed by the Bonferroni posttest. Comparison between several means was analyzed by 1-way ANOVA followed by the Tukey posttest. Comparison between 2 means was performed by 2-tailed Student *t* test or Mann-Whitney *U* test. Analyses were performed with GraphPad Prism 7 software (La Jolla, CA). Values of $P<0.05$ were accepted as statistically significant.

Human Data

Comparison of baseline characteristics between the 2 study groups (patients with moderate to severe AS and patients with no AS) was performed with the Student *t* test for continuous variables and the χ^2 test and Fisher exact test for categorical variables. The 2 groups were followed up through June 30, 2019, for the occurrence of nonhematologic cancer. Cox proportional hazard regression models were used to assess the univariate and the multivariate associations between moderate to severe AS and cancer. Models were adjusted for age, sex, ethnicity, socioeconomic status, alcohol abuse, smoking, obesity, diabetes mellitus, history of cancer, and aspirin and statin use. Post hoc analysis was performed in prespecified age subgroup (40–60 years versus ≥60 years). No correction was made for multiple testing because the post hoc analysis was considered an exploratory hypothesis-generating analysis.

The Major Resources Table in Methods in the Data Supplement provides more details.

RESULTS

Cardiac Remodeling Promotes Tumor Growth

Pressure overload and volume overload induce cardiac remodeling processes in the heart.[25] Cardiac remodeling is an adaptive process at its early stages, which

then turns into a maladaptive process leading to HF and death.[26] Here, we studied whether early cardiac remodeling processes affect noncardiac tissue pathology. We used TAC to induce pressure overload in C57Bl/6 female mice. Naive mice (control) and sham-operated mice (sham) served as control groups (Figure 1A). Ten days after TAC procedure, before the occurrence of major cardiac remodeling processes, we challenged the mice with a breast cancer PyMT orthotopic model. Tumor growth was monitored over time until the experiment reached humane end point (Figure 1A). We detected increased tumor volume in TAC-operated mice (1460±185.3 mm^3) compared with tumors implanted in control (1082.8±224.9 mm^3) and sham-operated mice (1001.2±87.5 mm^3; Figure 1B). Control and sham-operated mice had a similar growth rate (Figure 1B), thus excluding the effect of surgery on tumor growth. To assess cardiac function after TAC, we used echocardiography 1 day before the end point. FS was calculated as the heart contraction ratio in diastole and systole (Table II in the Data Supplement). Both naive and sham control groups displayed normal cardiac function, but the FS of TAC-operated mice was significantly decreased (Figure IIIA in the Data Supplement). TAC-operated mice displayed increased heart weight/body weight (HW/BW) ratio compared with control and sham-operated mice, indicating hypertrophy of the heart (Figure IIIB in the Data Supplement). Consistently, the increase in heart size after TAC was accompanied by elevated mRNA levels of hallmark hypertrophic markers such as *ANP*, *BNP*, β*MHC*, and *ACTA1* (Figure IIIC in the Data Supplement). Nonetheless, no cardiac fibrosis was detected with Masson trichrome staining (Figure IIID in the Data Supplement). Collectively, TAC-operated mice displayed mild cardiac remodeling and hypertrophy phenotype with reduced contractile function, with no signs of HF. Consistent with tumor volume measurements, tumors of TAC-operated mice were heavier compared with control and sham-operated mice (Figure 1C). In this experimental design, at the end point, we did not detect metastatic lesions in the lungs.

Next, we examined the effect of cardiac remodeling on tumor growth in male mice using a xenograft lung cancer model (Figure 1E). TAC-operated and control mice were implanted subcutaneously into the flank with LLC cells 17 days after TAC operation to have an experimental length comparable to that of the PyMT-TAC model (Figure 1E). TAC-operated mice displayed a typical cardiac remodeling phenotype as appreciated by reduced contractile function, increased HW/BW ratio, and elevated levels of hypertrophic gene signature (Figure IIIE through IIIG and Table III in the Data Supplement) with no sign of cardiac fibrosis (Figure IIIH in the Data Supplement) or HF. Similar to PyMT tumors, the growth rate of the LLC tumor volume was significantly higher in TAC-operated mice (control: 1345.6±275.4 mm^3; TAC: 1999±304 mm^3; Figure 1F). In addition, tumors from TAC-operated mice were heavier than sham-operated tumors (Figure 1G). In this experimental design, we did not detect metastatic lesions in the lungs.

To understand whether the tumor-promoting growth phenotype found in TAC-operated mice is the

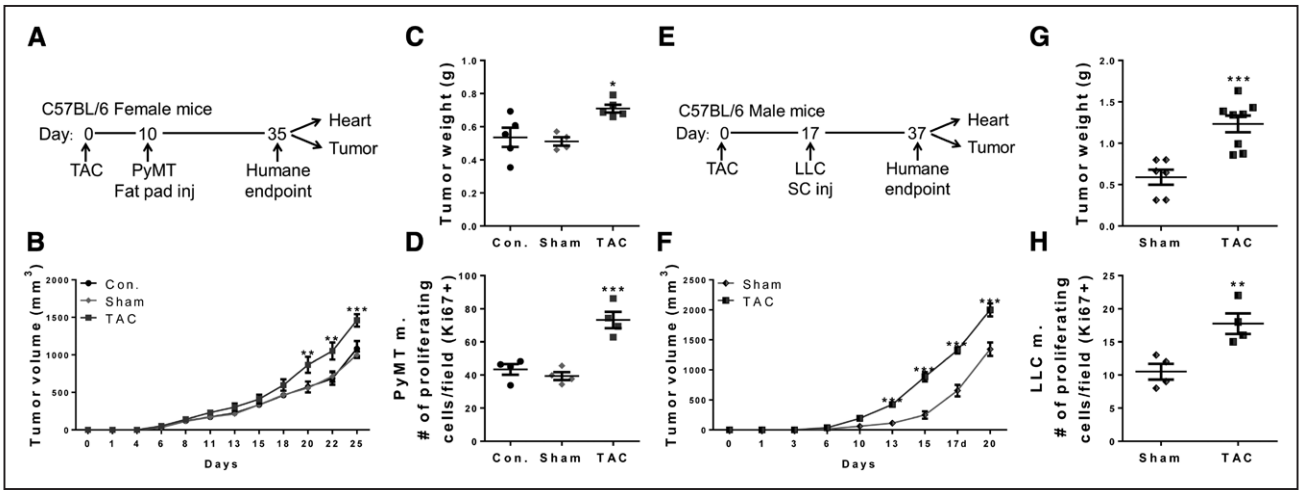

Figure 1. Transverse aortic constriction (TAC) enhances tumor growth.
A, A schematic diagram of the polyoma middle T (PyMT) cell model in female mice with control (Con.; n=5), sham (n=4) or TAC (n=5) operation after PyMT cancer cell injection (inj). **B**, Control, sham, and TAC-operated mice were orthotopically implanted into the mammary fat pad with PyMT cells (10^5 cells per mouse). Tumor volume was monitored over time with the following formula: $Width^2 \times Length \times 0.5$. **C**, Tumor weight at the end point. Each dot represents 1 mouse. **D,** Quantification of the number of proliferating cells ($Ki67^+$) in the tumor sections derived from control, sham, or TAC-operated mice. Each dot represents the mean of 5 random fields taken from 1 mouse. Data are presented as mean±SE. Representative image of at least three experiments. Two-way repeated-measures ANOVA followed by Bonferroni posttests (**B**) or 1-way ANOVA followed by Tukey posttests (**C** and **D**). **P*<0.05. ***P*<0.01. ****P*<0.001. **E**, A schematic diagram of the Lewis lung carcinoma (LLC) model in male mice with sham (n=6) or TAC (n=8) operation after subcutaneous implantation into the flanks with LLC cells (0.5×10^6 cells per mouse). **F**, Tumor volume was monitored over time and analyzed as described in **B**. **G**, Tumor weight at the end point. Each dot represents 1 mouse. **H**, Quantification of the number of proliferating cells ($Ki67^+$) in the tumor sections. Each dot represents the mean of 5 random fields taken from 1 mouse. Data are presented as mean±SE. Representative image of at least three experiments. Two-way repeated-measures ANOVA followed by Bonferroni posttests (**F**) or Student *t* test (**G** and **H**). ***P*<0.01. ****P*<0.001.

result of angiogenesis or increased cell proliferation, we immunostained PyMT and LLC tumor sections with anti-CD31 (endothelial cell marker). This analysis revealed no substantial differences in the area of blood vessels per field between tumor sections of all groups (Figure IVA through IVD in the Data Supplement). In contrast, Ki67 staining (cell proliferation marker) indicated a higher number of proliferating cells per field in tumor sections of TAC-operated mice compared with either control or sham-operated mice (Figure 1D and 1H and Figure IVE and IVF in the Data Supplement).

To gain further insights into the connection between cardiac remodeling and tumor growth at more advanced stages of cardiac remodeling, we implanted PyMT cancer cells 30 days after TAC operation (Figure VA in the Data Supplement). Although heart function as monitored by FS deteriorated only mildly with time compared with the previous model (Figure IIIA in the Data Supplement), an increase in HW/BW ratio and hypertrophic markers was readily detected at 55 days after TAC (Figure VB through VD in the Data Supplement). Consistently, the tumors of TAC-operated mice, implanted 30 days after surgery were larger than those implanted 10 days after the operation (30 days: 1746.4±157.3 mm^3; 10 days: 1460±185.3 mm^3; Figure VE and VF in the Data Supplement). We identified a linear correlation between the severity of cardiac remodeling parameters after TAC (ie, HW/BW ratio, *ANP* and *BNP*) and tumor weight (Figure VIA through VIC in the Data Supplement). Overall, these results emphasize a tight connection between cardiac remodeling severity and tumor growth.

Cardiac Remodeling Promotes Metastasis Colonization in the Lungs

Because of the relatively short time of the experimental models we used so far, we were unable to identify lung metastases in both PyMT and LLC cancer cell models. To examine whether cardiac remodeling affects metastasis to the lungs, we used an experimental metastasis assay in which cancer cells were injected directly into the tail vein of control and TAC-operated mice (Figure 2A and 2E). Similar to our previous results, TAC-operated mice displayed a cardiac remodeling phenotype, shown by an increased HW/BW ratio, and elevated levels of hypertrophic markers (Figure VIIA through VIID in the Data Supplement). Lung sections from TAC-operated mice displayed more cancer cell lesions with a larger area for both PyMT and LLC models (Figure 2B through 2D and Figure 2F through 2H). These results suggest that cardiac remodeling not only promoted cancer growth but also increased the number and size of tumor cell lesions in the lungs.

Increased Tumor Growth After TAC Is Not Mediated by Immune System Alterations

Our model suggests a connection between distinct and remote diseases that involve systemic processes such as immune processes and secreted proteins. We therefore investigated the possible involvement of the immune system in cardiac remodeling–dependent tumor growth. Using flow cytometry, we did not detect any significant changes in the percentage of major immune cell populations or in T-cell activation in the blood or tumor (Figure VIIIA through VIIF and Figure IXA through IXC in the Data Supplement). To further exclude the possible involvement of the immune system, we used the immunodeficient NOD/SCID mouse model in which mice exhibit deficiencies of lymphoid and nonfunctional myeloid cells.[27] We implanted PyMT cells in either TAC-operated or control NOD/SCID mice and monitored tumor growth over time (Figure 3A). Similar to the phenomenon we observed in C57Bl/6 mice, TAC-operated NOD/SCID mice displayed a significant increase in cardiac remodeling phenotype as indicated by reduced FS, increased HW/BW ratio, and elevated levels of hypertrophic gene signature with no sign of fibrosis (Figure 3B and 3C and Figure X and Table V in the Data Supplement). Tumors derived from NOD/SCID TAC-operated mice were larger in both volume and weight than those of control mice (TAC: 1746.4±157.3 mm^3; control: 1344.9±196.5 mm^3; Figure 3D and 3E). Collectively, increased tumor growth after TAC in immune-deficient mice excludes the significant involvement of major immune cell populations in this process.

Secreted Proteins in the Serum of TAC-Operated Mice Potentiate Cancer Cell Proliferation

To identify possible mediators of the TAC-induced tumor growth, we examined whether blood serum derived from TAC-operated mice can enhance cancer cell proliferation in vitro. To this end, PyMT and LLC cells were cultured in the presence of 10% mouse serum derived from naive, control, sham, or TAC-operated mice, tumor bearing or non–tumor bearing. Cell proliferation was monitored with luminescent cell viability assay after 24 and 48 hours, revealing that serum derived from TAC-operated mice increased both PyMT and LLC cell proliferation in vitro (Figure 4A and 4B and Figure XI in the Data Supplement). These results point to the presence of cell proliferation factors in the serum, potentially derived from the remodeled heart.

To identify whether and which tumor supporting factors are secreted by the remodeled heart, we compared RNA-seq data derived from hearts of non–tumor-bearing control, sham, and TAC-operated mice (Figure 4C and Table I in the Excel File in the Data

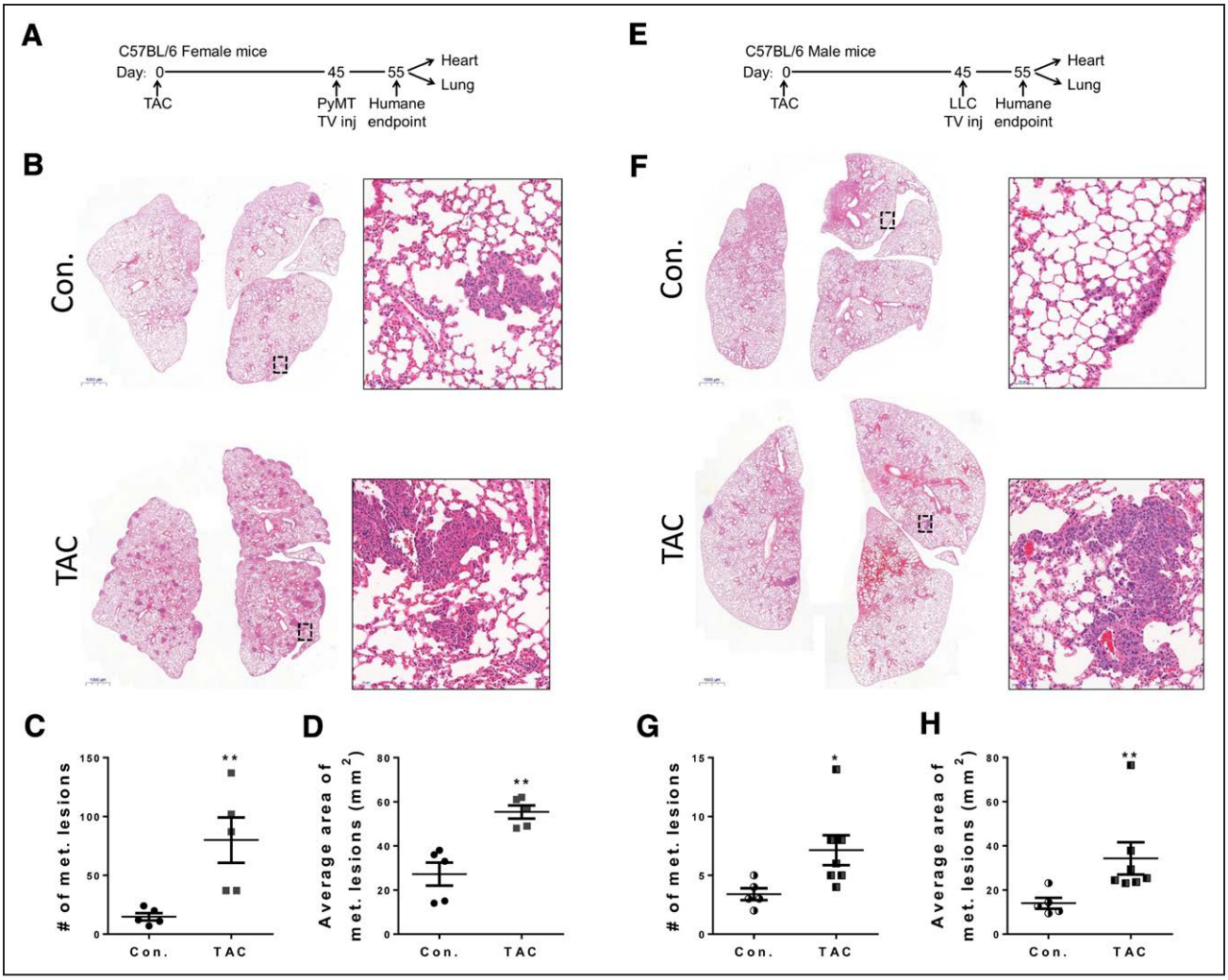

Figure 2. Transverse aortic constriction (TAC) enhances metastasis colonization in the lungs.
A, A schematic diagram describing TAC operation followed by polyoma middle T (PyMT) cell experimental metastasis assay (tail vein injection of 2×10^5 cells per mouse) in control (Con.; n=5) or TAC-operated (n=5) female mice. **B**, Representative images of lung sections stained with hematoxylin and eosin (H&E). Scale bar, 1000 and 50 µm. **C**, Number of metastatic lesions in the lung. **D**, Average area of the metastatic lesions. **E**, Schematic diagram describing TAC operation followed by the Lewis lung carcinoma (LLC) experimental metastasis assay (tail vein injection of 2×10^6 cells per mouse) in control (n=5) or TAC-operated (n=7) male mice. **F**, Representative images of lung sections stained with H&E. Scale bar, 1000 and 50 µm. **G**, Number of metastatic lesions in the lung. **H**, Average area of the metastatic lesions. Data are presented as mean±SE. Each dot represents 1 mouse. Mann Whitney *U* test (**C** and **H**) and Student *t* test (**D** and **G**). **P*<0.05. ***P*<0.01.

Supplement). The samples of control and sham-operated mice were clustered together, and the major effect was the result of TAC surgery. Gene analysis was performed according to the flow diagram depicted in Figure 4E. We identified 520 differentially expressed genes, of which 412 genes were upregulated and 108 genes were downregulated after TAC (Figure 4D). Using Gene Ontology, we annotated 395 of the 412 upregulated genes, and 59 of them were related to cell proliferation (Figure XII in the Data Supplement). Carcinoma- and lung cancer–associated pathways were ranked as the highest score–associated pathways (first and fourth, respectively) in the hearts of non–tumor-bearing mice after TAC operation (Figure XIII in the Data Supplement). Next, we classified 33 genes encoding for secreted proteins, which were upregulated after TAC (Table VI in the Data Supplement). These genes include *ANP*, *CTgF*, and *Periostin* (all 3 genes displayed a >2.5 fold increase; Figure 4E). *ANP* is a known cardiac hypertrophic marker[28] that was upregulated in all TAC-operated mice. *CTgF* and *Periostin* are known to play key roles in cancer progression.[29–31]

To further validate the RNA-seq results in our experimental setting, we examined the mRNA levels of *CTgF* and *Periostin* in the heart by quantitative polymerase chain reaction. Consistently, we found that *CTgF* and *Periostin* transcription was elevated in TAC-operated mice compared with control mice independently of cancer (Figure 4F and 4G). Moreover, we found elevated protein levels of CTgF and periostin in the serum of TAC-operated mice (Figure 5A and 5B). Because periostin levels in the serum were significantly higher than CTgF levels (microgram versus nanogram range, respectively), we next examined the

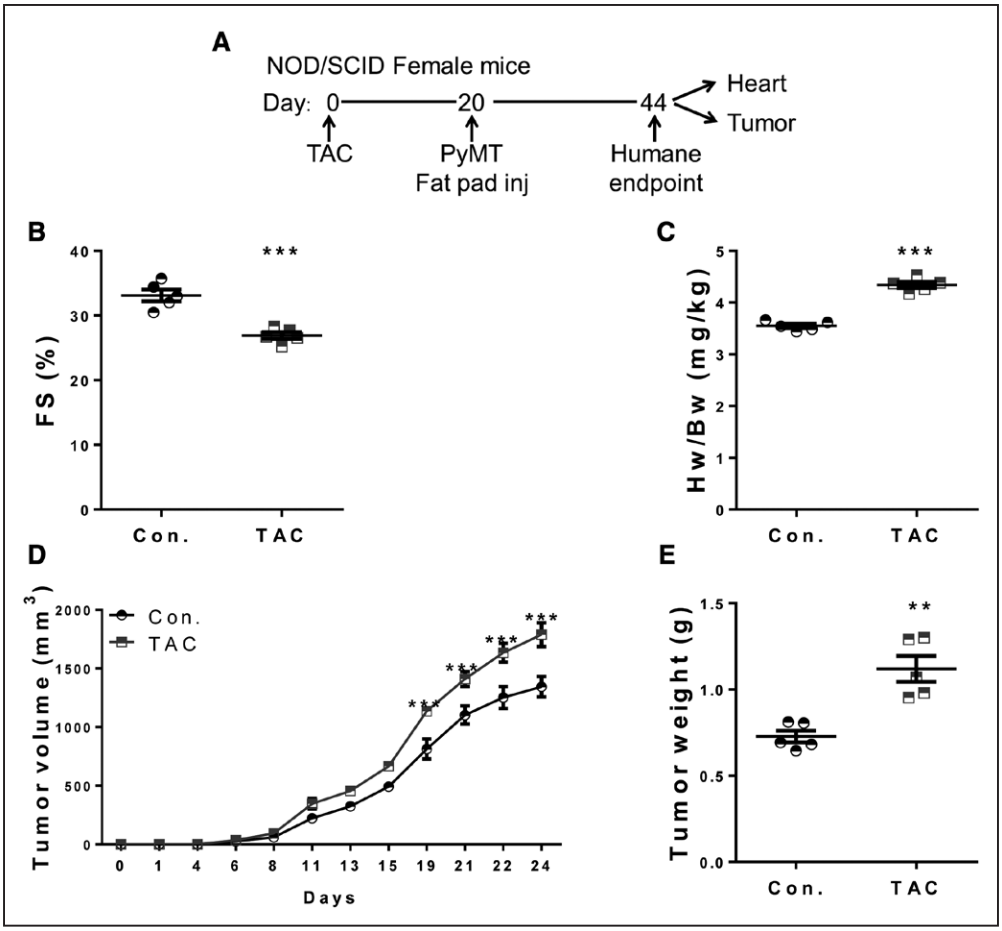

Figure 3. Transverse aortic constriction (TAC) enhances tumor growth in NOD/SCID (nonobese diabetic/severe combined immunodeficiency) mice. **A**, Schematic diagram of the polyoma middle T (PyMT) cell model in immunodeficient NOD/SCID female mice with control (Con.; n=5) or TAC (n=5) operation starting 20 days before PyMT cancer cell injection (inj). One day before the end point, mouse hearts were examined by echocardiography. **B**, Fractional shortening (FS). **C**, Heart weight/body weight (Hw/Bw) ratio. **D**, Control and TAC-operated mice were orthotopically implanted into the mammary fat pad with PyMT cells (1×10^5 cells per mouse). Tumor volume was monitored over time and analyzed as described in Figure 1. **E**, Tumor weight at the end point. Data are presented as mean±SE. Each dot represents 1 mouse. Two-way repeated-measures ANOVA followed by Bonferroni posttests (**D**) or Student *t* test (**B**, **C**, and **E**). ***P*<0.01. ****P*<0.001.

role of periostin and cancer cell proliferation in vitro. As shown in previous studies,[32,33] periostin addition to the media of PyMT or LLC cell cultures increased cell proliferation in a dose-dependent manner (Figure 5C and 5D). Moreover, periostin-depleted serum derived from TAC-operated mice did not increase PyMT cell proliferation in vitro (Figure 5E). Taken together, these results suggest that periostin and possibly CTgF secretion from the early remodeled heart can mediate the increase in tumor cell proliferation.

Cardiac Remodeling Per Se Promotes Tumor Growth

To examine whether mechanical stress caused by pressure overload or cardiac remodeling is responsible for increased tumor growth, we performed TAC and PyMT cancer cell implantation in a genetically modified mouse strain resistant to maladaptive cardiac remodeling (MCRR)[17] (Figure 6A). As expected, MCRR mice displayed no cardiac remodeling phenotype according to their FS, HW/BW, and hypertrophic markers (Figure 6B through 6D and Table VII in the Data Supplement). In addition, TAC-operated MCRR mice and control mice displayed similar tumor growth rates (Figure 6E and 6F). *Periostin* and *CTgF* mRNA and protein levels were similar in TAC-operated and control MCRR mice, in the heart and in the serum, respectively, which was in accordance with the inability of TAC to promote cancer growth in this mouse model (Figure 6G and 6H). Collectively, these results suggest that intrinsic early cardiac remodeling processes are responsible for the increase in tumor growth.

Association Between AS and Cancer Risk

TAC is an experimental model for pressure overload–induced cardiac hypertrophy, which also occurs in AS in humans. To address the relevance of our study to human disease, we studied echocardiography data of

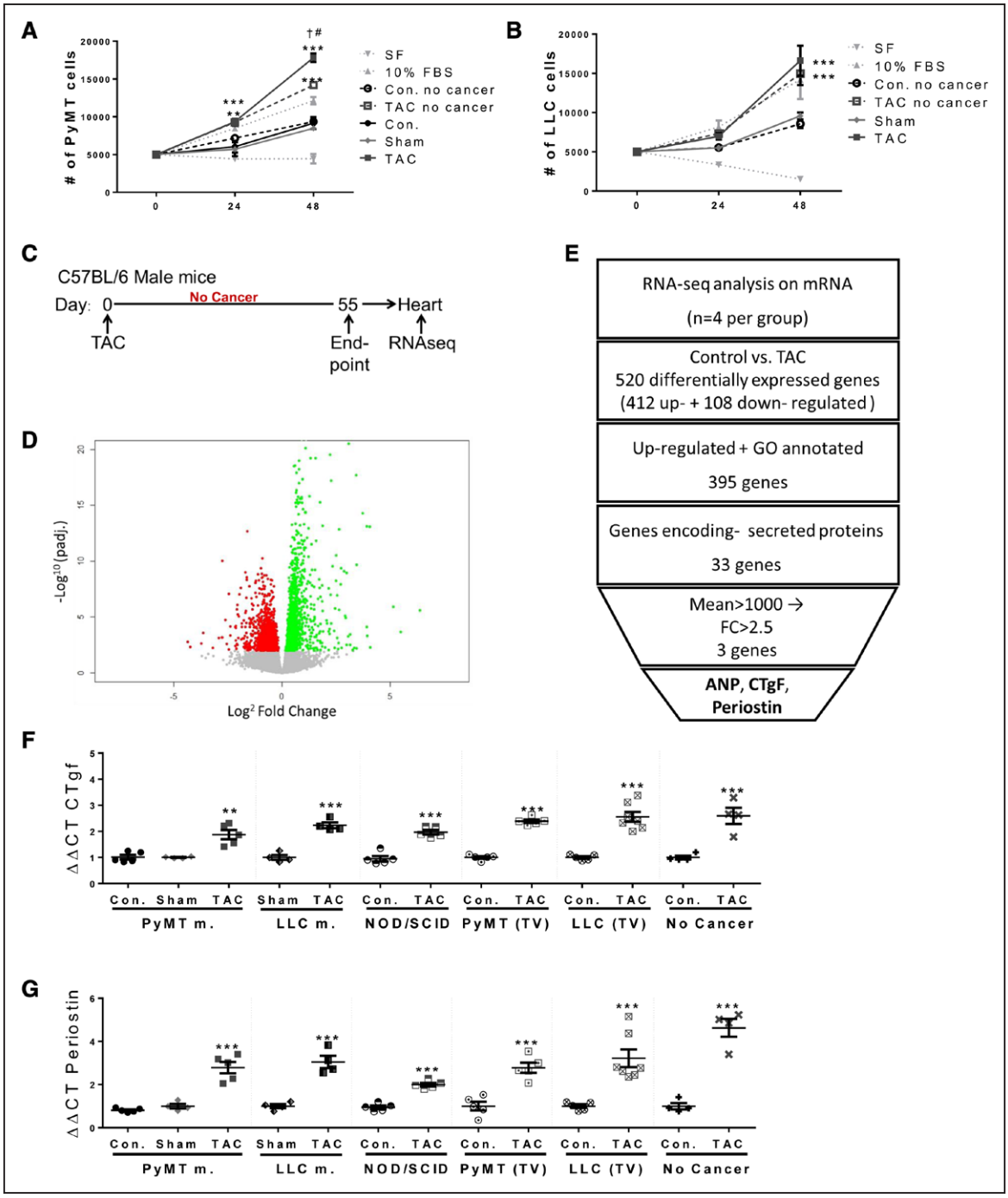

Figure 4. Serum of transverse aortic constriction (TAC)–operated mice increases cancer cell proliferation in vitro.
A and **B**, Polyoma middle T (PyMT; **A**) and Lewis lung carcinoma (LLC; **B**) cells were cultured in 10% FBS, serum free (SF), or 10% mouse serum of naive, control, sham, or TAC-operated non–tumor-bearing or tumor-bearing mice from the PyMT (**A**) or the LLC (**B**) models for 24 and 48 hours. Proliferation rate was measured with the Luminescent Cell Viability Assay; n=4 plates per treatment per time point. Data are presented as mean±SE. Representative image of at least 3 experiments. Two-way ANOVA followed by Bonferroni posttests: difference between mouse treatments, ***P*<0.01 and ****P*<0.001; †difference compared with 10% FBS; #difference compared with non–tumor-bearing TAC-operated mice. **C**, Schematic diagram of the RNA-sequencing (RNA-seq) experiment. Control (Con.; n=4; 2 Con.+ 2 sham) and TAC-operated (n=4) cancer-free male mice. **D**, Volcano plot of the total RNA-seq depicting the fold difference in gene expression levels. Red dots represent downregulated genes; green dots represent upregulated genes according to their log fold change in *x* axis and adjusted *P* value (log^{10} $P_{adjusted}$) $P_{adjusted}$<0.01 in *y* axis. **E**, Flowchart of the steps taken to identify novel cardiac remodeling genes encoding for secreted proteins. **F** and **G**, mRNA levels of connective tissue growth factor (CTgF; **F**) and periostin (**G**) in the hearts of mice from the PyMT, LLC, NOD/SCID (nonobese diabetic/severe combined immunodeficiency), tail vein injection models, and non–tumor-bearing mice, determined by quantitative polymerase chain reaction. Data are presented as relative expression compared with control or sham determined as 1. Data are presented as mean±SE. One-way ANOVA followed by Tukey posttests or multiple Student *t* tests. ***P*<0.01. ****P*<0.001.

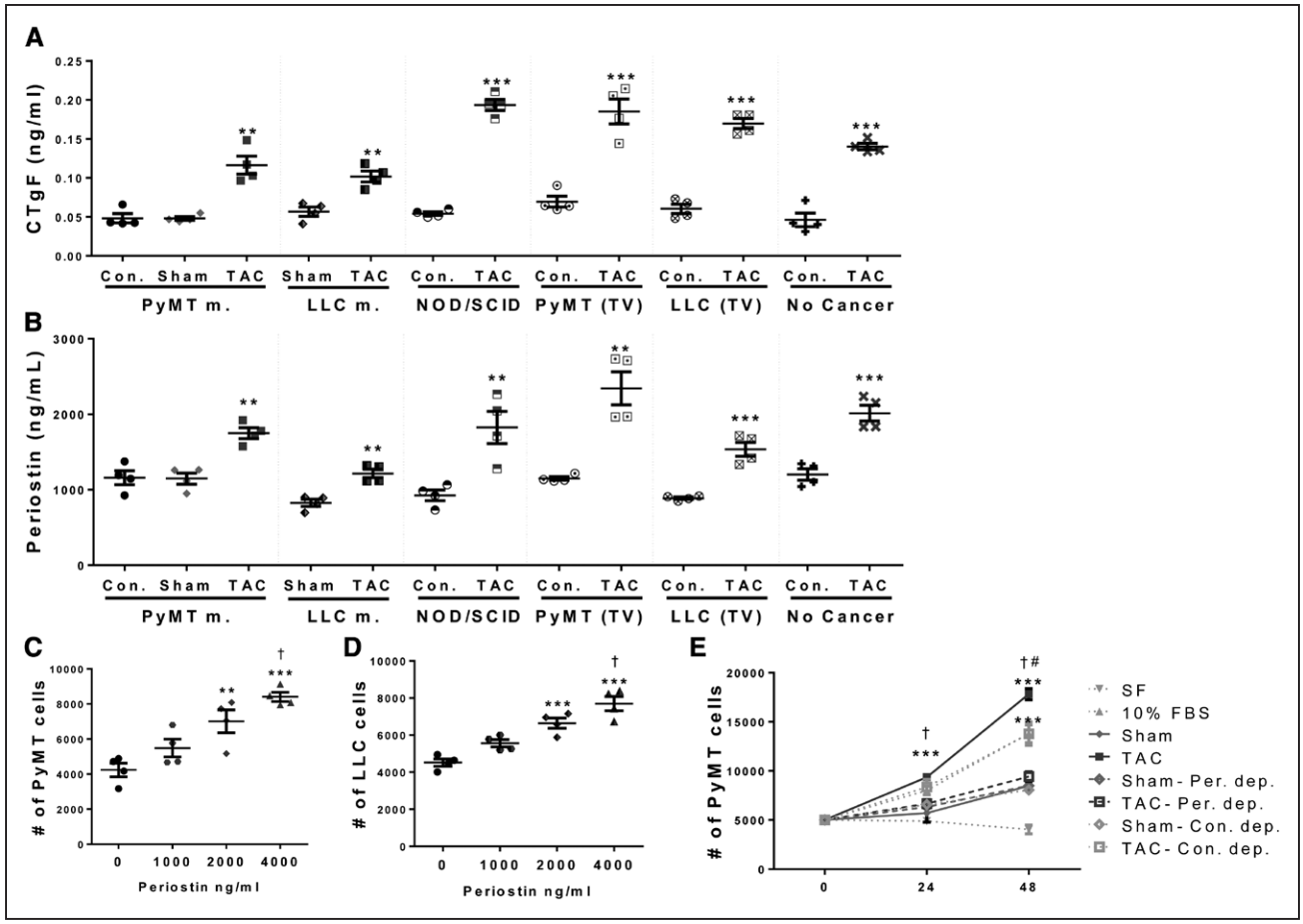

Figure 5. Periostin depletion abrogates cancer cell proliferation in vitro.
A and **B**, Protein levels of connective tissue growth factor (CTgF; **A**) and periostin (**B**) in the blood serum of mice from the polyoma middle T (PyMT), Lewis lung carcinoma (LLC), NOD/SCID (nonobese diabetic/severe combined immunodeficiency), tail vein injection models, and non–tumor-bearing mice, determined by ELISA. Data are presented as mean±SE. One-way ANOVA followed by Tukey posttests or multiple Student *t* tests. ***P*<0.01. ****P*<0.001. PyMT (**C**) and LLC (**D**) cells were cultured in 1% FBS supplemented with 1000, 2000, or 4000 ng/mL periostin for 48 hours. Proliferation rate was measured as described in Figure 4. Data are presented as mean±SE. One-way ANOVA followed by Tukey posttests or multiple Student *t* tests. Difference compared with control (0 ng/mL),** *P*<0.01, ****P*<0.001; †difference compared with 1000 ng/mL **E**, PyMT cells were cultured in 10% of FBS, serum-free (SF), or 10% blood serum of sham or TAC-operated mice from the PyMT models after control immunodepletion (Con. Dep.) or periostin immunodepletion (Per. Dep.) for 24 and 48 hours. Proliferation rate was measured as described in Figure 4. Data are presented as mean±SE. Two-way ANOVA followed by Bonferroni posttests. Difference between mouse treatments, ****P*<0.001; †difference compared with 10% FBS; #difference compared with TAC-Con. dep.

patients and followed them up for cancer diagnosis thereafter. A total of 80723 patients were included in the study (75800 with no AS and 4923 with moderate to severe AS; Table VIII in the Data Supplement). Overall, 8277 new nonhematologic cancers were diagnosed during a median follow-up of 5.4 years (interquartile range, 2.4–8.8 years). The crude incidence rate (Table) and the cumulative death (Figure XIV in the Data Supplement) of cancer were higher in patients with moderate to severe AS than in patients with no AS. After further adjustment for age, ethnicity, alcohol abuse, smoking, obesity, diabetes mellitus, history of cancer, and aspirin and statin use, there was no significant association between moderate to severe AS and cancer (hazard ratio, 1.00 [95% CI, 0.91–1.09]; *P*=0.929). However, a post hoc analysis within a prespecified age groups showed a significant interaction between age and AS ($P_{interaction}$<0.001) with a significant association in patients 40 to 60 years of age (hazard ratio, 1.64 [1.14–2.36], *P*=0.008) but not in patients >60 years of age (hazard ratio, 1.00 [95% CI, 0.91–1.11]; *P*=0.913; Table and Table IX in the Data Supplement). Thus, we hypothesize that AS may be associated with increased risk of cancer in 40- to 60-year-old patients.

DISCUSSION

Cardiac remodeling is an adaptive response that may turn into a maladaptive process, leading to heart hypertrophy and contractile dysfunction. Reduced muscle contractility is caused mainly by muscle dilatation and fibrosis, resulting in a vicious cycle that eventually leads to HF and death. Although it has been shown that myocardial infarction–induced HF promotes cancer progression,[16] thus far, data have not been available on the early stages of cardiac remodeling before HF.

ORIGINAL RESEARCH ARTICLE

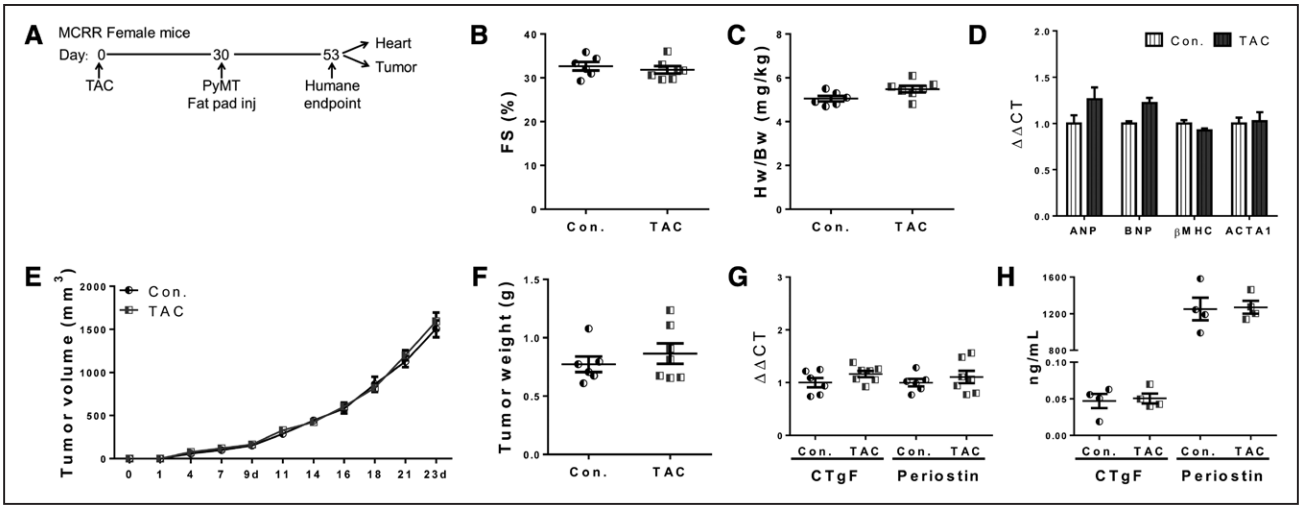

Figure 6. Transverse aortic constriction (TAC)–enhanced tumor growth is abrogated in the maladaptive cardiac remodeling–resistant (MCRR) mouse model.

A, A schematic diagram of the polyoma middle T (PyMT) cell model in female MCRR mice with control (Con.; n=6) or TAC (n=7) operation after PyMT cancer cell injection (inj). **B**, Fractional shortening (FS). **C**, Heart weight/body weight (Hw/Bw) ratio. **D**, mRNA levels of the hypertrophy markers ANP (atrial natriuretic peptide), BNP (brain natriuretic peptide), β-myosin heavy chain (βMHC), and ACTA1 were determined by quantitative polymerase chain reaction. **E**, Control and TAC-operated mice were orthotopically implanted into the mammary fat pad with PyMT cells (1×10^5 cells per mouse). Tumor volume was monitored over time and analyzed as described in Figure 1. **F**, Tumor weight at the end point. **G**, mRNA levels of *CTgF* and *Periostin* in the heart. **H**, Protein levels of connective tissue growth factor (CTgF) and periostin in the serum. Each dot represents 1 mouse. Data are presented as mean±SE. Student *t* test (**B**, **C**, and **F**), multiple Student *t* tests (**D**, **G**, and **H**) or 2-way repeated-measures ANOVA (**E**).

Here, we studied TAC in mice, a model for pressure overload–induced cardiac hypertrophy; this is one of the processes occurring in AS in humans in which the narrowing of the aortic valve results in pressure overload.[34] The narrowing of the aortic valve occurs gradually and may take a decade before reaching a severe stage, in which valve replacement surgery is performed to prevent HF.[35] Although AS is treated symptomatically and considered a local disease of the heart, limited information is available on the effects of the remodeled heart on other organs. Studies have shown that patients with cancer and AS display a poorer prognosis compared with patients with cancer without AS.[36,37] Treating AS by aortic valve replacement did not improve the prognosis of patients with cancer,[38] further indicating the importance of early detection and treatment of early cardiac remodeling. The crude analysis in our study showed that patients with AS are more prone to develop nonhematologic cancers. Extensive analysis revealed that the higher incidence is caused mainly by common risk factors for both cardiac disease and cancer (smoking, obesity, diabetes mellitus, and others).[39] However, in a post hoc analysis, we found that in the subgroup of patients 40 to 60 years of age, AS is a significant risk factor for nonhematologic cancers. It must be noted that the subgroup was based on a

Table. AS Is Associated With Increased Risk of Cancer in Younger Patients

AS Status	Events, n	Follow-Up, Person-Year	Incidence Rate, per 1000 Patient-Year	Crude Hazard Ratio (95% CI)	Adjusted* Hazard Ratio (95% CI)
Entire study population (n=80 723)					
Moderate to severe AS (n=4923)	494	20 746	23.8	1.33 (1.21–1.46)	1.00 (0.91–1.09)
No AS (n=75 800)	7783	450 972	17.3	Reference	Reference
Age 40–60 y (n=23 266)					
Moderate to severe AS (n=285)	30	1869	16.0	1.71 (1.19–2.46)	1.64 (1.14–2.36)
No AS (n=22 981)	1464	156 885	9.3	Reference	Reference
Age ≥60 y (n=57 457)					
Moderate to severe AS (n=4638)	464	18 877	24.6	1.11 (1.01–1.22)	1.00 (0.91–1.11)
No AS (n=52 819)	6319	294 088	21.5	Reference	Reference

Crude incidence rate of nonhematologic cancers according to AS status and crude and adjusted hazard ratios presented separately for the entire study group and by age group (40–60 years versus ≥60 years).

AS indicates aortic stenosis.

*Adjusted for age (continuous variable), sex, ethnicity, socioeconomic status, smoking, alcohol abuse, obesity, diabetes mellitus, history of cancer, aspirin use, and statin use.

relatively small number of patients with AS (n=285) including only 30 events. Therefore, these results should be interpreted with caution and should be considered hypothesis-generating findings that need to be replicated in a new data set.

We excluded the effect of surgery on tumor growth by using sham-operated mice, which had a tumor growth similar to that of naive mice. Although previous studies demonstrated that surgery promotes remodeling of the lung,[40] the effects were found to last for a relatively short period of time (up to 72 hour). In our study, TAC surgery was performed at least 10 days before mice were subjected to tumor cell implantation, therefore eliminating the possible effect of surgery on lung tumor cell seeding. In addition, the TAC-associated increase in cancer progression was independent of immune system alterations because we did not detect any significant changes in the percentage of tumor or blood immune cell populations between groups. This was a surprising result because both cardiac remodeling and cancer are known to be modulated by immune cells and inflammatory processes.[1,7,41] Nonetheless, TAC-operated NOD/SCID mice lacking B cells, T cells, and functional myeloid cells showed an increase in tumor growth similar to the increase we showed in TAC-operated C57Bl/6 mice.

Subsequently, we identified that the cardiac remodeling–dependent tumor growth was regulated, at least in part, by secreted factors in the blood. Serum derived from TAC-operated mice induced cancer cell proliferation in vitro. Our RNA-seq analysis of heart tissue identified *Periostin* and *CTgF* as putative factors that may affect tumor cell proliferation and metastatic lesions. Indeed, the levels of both periostin and CTgF were elevated in blood serum after TAC. Both factors are known to be extracellular matrix proteins that affect cancer cell proliferation and migration and epithelial to mesenchymal transition.[29,31,42,43] Accordingly, periostin-depleted serum derived from TAC-operated mice abrogated the increase in cell proliferation. Conversely, periostin also increased cell proliferation in vitro. The upregulation of *Periostin* and *CTgF* in the heart after TAC may further emphasize the connection of cardiac remodeling and tumor growth.

Using a pulmonary metastasis assay, we demonstrated that TAC operation likely contributed to tumor cell seeding and expansion in the lungs, reinforcing the results of the primary tumors. This improved seeding of cancer cells in the lungs of TAC-operated mice can be attributed to the secretion of periostin and CTgF because they are key factors in the progression of metastatic lesions by affecting cell mobility and adhesion.[44–46]

A previous study identified that myocardial infarction (HF mouse model) in a genetic spontaneous intestinal adenoma formation model promotes intestinal tumor load.[16,47,48] The authors identified a total of 5 secreted proteins that may affect the observed increase in tumor load and ultimately proposed serpin3a as the major factor that induces the tumor progression effect.[16] We tested all 5 factors in the hearts of our TAC-operated mice but did not detect changes in their expression compared with control mice. This suggests an altered gene expression signature of secreted factors between early and late stages of cardiac remodeling and HF. We specifically used an early, pre-HF, cardiac remodeling paradigm to demonstrate that early cardiac remodeling is sufficient to promote cancer progression.

We further investigated whether the tumor growth-promoting effects result from the intrinsic remodeling of the heart or originate from the constriction of the aorta and perturbation. First, we showed a linear correlation between multiple cardiac remodeling hallmark phenotypes and tumor weight. Second, to distinguish between tumor growth after TAC operation in the presence or absence of cardiac remodeling, we used the MCRR mouse strain. Indeed, MCRR TAC-operated mice displayed no cardiac remodeling and did not have any differences in tumor growth compared with control MCRR mice. This strain enabled us to provide evidence that cardiac remodeling per se is responsible for increased tumor growth. Consistently, the lack of increased levels of periostin and CTgF in TAC-operated MCRR mice matched the failure to promote cancer growth.

Collectively, our study suggests that early stages of cardiac remodeling before HF promote cancer progression. Our data highlight the importance of diagnosis and treatment at the early stages of cardiac remodeling because it may attenuate cancer onset and ameliorate cancer outcome.

ARTICLE INFORMATION

Received February 25, 2020; accepted May 8, 2020.

The Data Supplement, podcast, and transcript are available with this article at https://www.ahajournals.org/doi/suppl/10.1161/circulationaha.120.046471.

Correspondence

Ami Aronheim, PhD, or Yuval Shaked, PhD, 7th Efron Street, Bat-Galim, PO Box 9649, Haifa, Israel 31096, Email aronheim@technion.ac.il or yshaked@technion.ac.il

Affiliations

Department of Cell Biology and Cancer Science (S.A., S.A.-S., R.K., T.F., Y.S., A.A.), Department of Immunology (B.K.), Department of Neuroscience (B.K.), The Ruth and Bruce Rappaport Faculty of Medicine (S.A., S.A.-S., R.K., T.F., Y.S., A.A., B.K., A.S., W.S.), and Pre-Clinical Research Authority Unit (R.S., T.H.), Department of Cardiovascular Medicine (A.S.), and Department of Community Medicine and Epidemiology (W.S.), Lady Davis Carmel Medical Center, Technion–Israel Institute of Technology, Haifa, Israel. Department of Cardiac Surgery (T.F.), Rambam Medical Center, Haifa, Israel.

Acknowledgments

The authors thank Professors Izhak Kehat, Dov Hershkovitz, and Asya Rolls and Dr Sharon Aviram for their support and helpful discussions. The authors also thank Dr Liat Linde for providing help and guidance in the RNA-seq analysis, Dr Edith Suss-Toby for her help with imaging analysis, and Drs Sagee Tal and Geulah Ben-David for editing the article. S.A. designed and carried out the mouse

experiments, analyzed and interpreted the results, and wrote the article. S.A.-S. helped with some of the in vivo experiments and performed part of the in vitro experiments. R.S. and T.H. performed all TAC operations and experimental metastasis assay. B.K. performed the flow cytometry analyses, contributed to the execution of mouse experiments, and revised the manuscript. R.K. performed the RNA-seq sample extraction and purification. T.F. helped to design the human data collection. A.S. designed the human data analysis and provided the echocardiography data. W.S. designed and performed the human data analysis. Y.S. and A.A. led the experimental design and interpretation of results and revised the article.

Sources of Funding

This work was supported by the Israel Science Foundation grant 731/17 to Dr Aronheim and in part by the European Research Council (#771112) to Dr Shaked.

Disclosures

None.

Materials

Expanded Methods
Data Supplement Figures I–XV
Data Supplement Tables I–IX
Excel File I

REFERENCES

1. Maillet M, van Berlo JH, Molkentin JD. Molecular basis of physiological heart growth: fundamental concepts and new players. *Nat Rev Mol Cell Biol.* 2013;14:38–48. doi: 10.1038/nrm3495
2. Bisping E, Wakula P, Poteser M, Heinzel FR. Targeting cardiac hypertrophy: toward a causal heart failure therapy. *J Cardiovasc Pharmacol.* 2014;64:293–305. doi: 10.1097/FJC.0000000000000126
3. Ganau A, Devereux RB, Roman MJ, de Simone G, Pickering TG, Saba PS, Vargiu P, Simongini I, Laragh JH. Patterns of left ventricular hypertrophy and geometric remodeling in essential hypertension. *J Am Coll Cardiol.* 1992;19:1550–1558. doi: 10.1016/0735-1097(92)90617-v
4. Maulik SK, Kumar S. Oxidative stress and cardiac hypertrophy: a review. *Toxicol Mech Methods.* 2012;22:359–366. doi: 10.3109/15376516.2012.666650
5. Carroll JF, Dwyer TM, Grady AW, Reinhart GA, Montani JP, Cockrell K, Meydrech EF, Mizelle HL. Hypertension, cardiac hypertrophy, and neurohumoral activity in a new animal model of obesity. *Am J Physiol.* 1996;271(pt 2):H373–H378. doi: 10.1152/ajpheart.1996.271.1.H373
6. Urena M, Webb JG, Eltchaninoff H, Muñoz-García AJ, Bouleti C, Tamburino C, Nombela-Franco L, Nietlispach F, Moris C, Ruel M, et al. Late cardiac death in patients undergoing transcatheter aortic valve replacement: incidence and predictors of advanced heart failure and sudden cardiac death. *J Am Coll Cardiol.* 2015;65:437–448. doi: 10.1016/j.jacc.2014.11.027
7. Koene RJ, Prizment AE, Blaes A, Konety SH. Shared risk factors in cardiovascular disease and cancer. *Circulation.* 2016;133:1104–1114. doi: 10.1161/CIRCULATIONAHA.115.020406
8. Hoshijima M, Chien KR. Mixed signals in heart failure: cancer rules. *J Clin Invest.* 2002;109:849–855. doi: 10.1172/JCI15380
9. Patel AP, Natarajan P. Completing the genetic spectrum influencing coronary artery disease: from germline to somatic variation. *Cardiovasc Res.* 2019;115:830–843. doi: 10.1093/cvr/cvz032
10. Hasin T, Gerber Y, Weston SA, Jiang R, Killian JM, Manemann SM, Cerhan JR, Roger VL. Heart failure after myocardial infarction is associated with increased risk of cancer. *J Am Coll Cardiol.* 2016;68:265–271. doi: 10.1016/j.jacc.2016.04.053
11. Hasin T, Gerber Y, McNallan SM, Weston SA, Kushwaha SS, Nelson TJ, Cerhan JR, Roger VL. Patients with heart failure have an increased risk of incident cancer. *J Am Coll Cardiol.* 2013;62:881–886. doi: 10.1016/j.jacc.2013.04.088
12. Sakamoto M, Hasegawa T, Asakura M, Kanzaki H, Takahama H, Amaki M, Mochizuki N, Anzai T, Hamasaki T, Kitakaze M. Does the pathophysiology of heart failure prime the incidence of cancer? *Hypertens Res.* 2017;40:831–836. doi: 10.1038/hr.2017.45
13. Banke A, Schou M, Videbaek L, Møller JE, Torp-Pedersen C, Gustafsson F, Dahl JS, Køber L, Hildebrandt PR, Gislason GH. Incidence of cancer in patients with chronic heart failure: a long-term follow-up study. *Eur J Heart Fail.* 2016;18:260–266. doi: 10.1002/ejhf.472
14. Daughaday WH, Deuel TF. Tumor secretion of growth factors. *Endocrinol Metab Clin North Am.* 1991;20:539–563.
15. Fountoulaki K, Dagres N, Iliodromitis EK. Cellular communications in the heart. *Card Fail Rev.* 2015;1:64–68. doi: 10.15420/cfr.2015.1.2.64
16. Meijers WC, Maglione M, Bakker SJL, Oberhuber R, Kieneker LM, de Jong S, Haubner BJ, Nagengast WB, Lyon AR, van der Vegt B, et al. Heart failure stimulates tumor growth by circulating factors. *Circulation.* 2018;138:678–691. doi: 10.1161/CIRCULATIONAHA.117.030816
17. Kalfon R, Friedman T, Eliachar S, Shofti R, Haas T, Koren L, Moskovitz JD, Hai T, Aronheim A. JDP2 and ATF3 deficiencies dampen maladaptive cardiac remodeling and preserve cardiac function. *PLoS One.* 2019;14:e0213081. doi: 10.1371/journal.pone.0213081
18. deAlmeida AC, van Oort RJ, Wehrens XHT. Transverse aortic constriction in mice. *J Vis Exp.* 2010;e1729:38. doi: 10.3791/1729
19. Wolford CC, McConoughey SJ, Jalgaonkar SP, Leon M, Merchant AS, Dominick JL, Yin X, Chang Y, Zmuda EJ, O'Toole SA, et al. Transcription factor ATF3 links host adaptive response to breast cancer metastasis. *J Clin Invest.* 2013;123:2893–2906. doi: 10.1172/JCI64410
20. Avraham S, Korin B, Aviram S, Shechter D, Shaked Y, Aronheim A. ATF3 and JDP2 deficiency in cancer associated fibroblasts promotes tumor growth via SDF-1 transcription. *Oncogene.* 2019;38:3812–3823. doi: 10.1038/s41388-019-0692-y
21. Chang YS, Jalgaonkar SP, Middleton JD, Hai T. Stress-inducible gene Atf3 in the noncancer host cells contributes to chemotherapy-exacerbated breast cancer metastasis. *Proc Natl Acad Sci USA.* 2017;114:E7159–E7168. doi: 10.1073/pnas.1700455114
22. Schneider CA, Rasband WS, Eliceiri KW. NIH Image to ImageJ: 25 years of image analysis. *Nat Methods.* 2012;9:671–675. doi: 10.1038/nmeth.2089
23. Liao Y, Wang J, Jaehnig EJ, Shi Z, Zhang B. WebGestalt 2019: gene set analysis toolkit with revamped UIs and APIs. *Nucleic Acids Res.* 2019;47:W199–W205. doi: 10.1093/nar/gkz401
24. UniProt Consortium. UniProt: a worldwide hub of protein knowledge. *Nucleic Acids Res.* 2019;47:D506–D515. doi: 10.1093/nar/gky1049
25. Mao Y, Tokudome T, Kishimoto I, Otani K, Nishimura H, Yamaguchi O, Otsu K, Miyazato M, Kangawa K. Endogenous ghrelin attenuates pressure overload-induced cardiac hypertrophy via a cholinergic anti-inflammatory pathway. *Hypertension.* 2015;65:1238–1244. doi: 10.1161/HYPERTENSIONAHA.114.04864
26. Gheorghiade M, Larson CJ, Shah SJ, Greene SJ, Cleland JGF, Colucci WS, Dunnmon P, Epstein SE, Kim RJ, Parsey RV, et al. Developing new treatments for heart failure. *Circ Heart Fail.* 2016;9:e002727.
27. Prochazka M, Gaskins HR, Shultz LD, Leiter EH. The nonobese diabetic scid mouse: model for spontaneous thymomagenesis associated with immunodeficiency. *Proc Natl Acad Sci U S A.* 1992;89:3290–3294. doi: 10.1073/pnas.89.8.3290
28. Knowles JW, Esposito G, Mao L, Hagaman JR, Fox JE, Smithies O, Rockman HA, Maeda N. Pressure-independent enhancement of cardiac hypertrophy in natriuretic peptide receptor A-deficient mice. *J Clin Invest.* 2001;107:975–984. doi: 10.1172/JCI11273
29. Chu CY, Chang CC, Prakash E, Kuo ML. Connective tissue growth factor (CTGF) and cancer progression. *J Biomed Sci.* 2008;15:675–685. doi: 10.1007/s11373-008-9264-9
30. Oatmen KE, Cull E, Spinale FG. Heart failure as interstitial cancer: emergence of a malignant fibroblast phenotype. *Nat Rev Cardiol.* 2020;17:523–531. doi: 10.1038/s41569-019-0286-y
31. Morra L, Moch H. Periostin expression and epithelial-mesenchymal transition in cancer: a review and an update. *Virchows Arch.* 2011;459:465–475. doi: 10.1007/s00428-011-1151-5
32. Tai IT, Dai M, Chen LB. Periostin induction in tumor cell line explants and inhibition of in vitro cell growth by anti-periostin antibodies. *Carcinogenesis.* 2005;26:908–915. doi: 10.1093/carcin/bgi034
33. Okazaki T, Tamai K, Shibuya R, Nakamura M, Mochizuki M, Yamaguchi K, Abe J, Takahashi S, Sato I, Kudo A, et al. Periostin is a negative prognostic factor and promotes cancer cell proliferation in non-small cell lung cancer. *Oncotarget.* 2018;9:31187–31199. doi: 10.18632/oncotarget.25435
34. Dweck MR, Joshi S, Murigu T, Gulati A, Alpendurada F, Jabbour A, Maceira A, Roussin I, Northridge DB, Kilner PJ, et al. Left ventricular remodeling and hypertrophy in patients with aortic stenosis: insights from cardiovascular magnetic resonance. *J Cardiovasc Magn Reson.* 2012;14:50. doi: 10.1186/1532-429X-14-50

35. Kupari M, Turto H, Lommi J. Left ventricular hypertrophy in aortic valve stenosis: preventive or promotive of systolic dysfunction and heart failure? *Eur Heart J.* 2005;26:1790–1796. doi: 10.1093/eurheartj/ehi290
36. Kornowski R. Transcatheter aortic valve replacement for oncology patients with severe symptomatic aortic stenosis: new hope for a complicated medical condition. *Catheter Cardiovasc Interv.* 2019;94:446–447. doi: 10.1002/ccd.28484
37. Landes U, Iakobishvili Z, Vronsky D, Zusman O, Barsheshet A, Jaffe R, Jubran A, Yoon SH, Makkar RR, Taramasso M, et al. Transcatheter aortic valve replacement in oncology patients with severe aortic stenosis. *JACC Cardiovasc Interv.* 2019;12:78–86. doi: 10.1016/j.jcin.2018.10.026
38. Peto R, Emberson J, Landray M, Baigent C, Collins R, Clare R, Califf R. Analyses of cancer data from three ezetimibe trials. *N Engl J Med.* 2008;359:1357–1366. doi: 10.1056/NEJMsa0806603
39. Meijers WC, de Boer RA. Common risk factors for heart failure and cancer. *Cardiovasc Res.* 2019;115:844–853. doi: 10.1093/cvr/cvz035
40. Rachman-Tzemah C, Zaffryar-Eilot S, Grossman M, Ribero D, Timaner M, Mäki JM, Myllyharju J, Bertolini F, Hershkovitz D, Sagi I, et al. Blocking surgically induced lysyl oxidase activity reduces the risk of lung metastases. *Cell Rep.* 2017;19:774–784. doi: 10.1016/j.celrep.2017.04.005
41. Bertero E, Ameri P, Maack C. Bidirectional relationship between cancer and heart failure: old and new issues in cardio-oncology. *Card Fail Rev.* 2019;5:106–111. doi: 10.15420/cfr.2019.1.2
42. Pandey DP, Lappano R, Albanito L, Madeo A, Maggiolini M, Picard D. Estrogenic GPR30 signalling induces proliferation and migration of breast cancer cells through CTGF. *EMBO J.* 2009;28:523–532. doi: 10.1038/emboj.2008.304
43. Liu Y, Liu BA. Enhanced proliferation, invasion, and epithelial-mesenchymal transition of nicotine-promoted gastric cancer by periostin. *World J Gastroenterol.* 2011;17:2674–2680. doi: 10.3748/wjg.v17.i21.2674
44. Finger EC, Cheng CF, Williams TR, Rankin EB, Bedogni B, Tachiki L, Spong S, Giaccia AJ, Powell MB. CTGF is a therapeutic target for metastatic melanoma. *Oncogene.* 2014;33:1093–1100. doi: 10.1038/onc.2013.47
45. Wang Z, Ouyang G. Periostin: a bridge between cancer stem cells and their metastatic niche. *Cell Stem Cell.* 2012;10:111–112. doi: 10.1016/j.stem.2012.01.002
46. Kudo Y, Ogawa I, Kitajima S, Kitagawa M, Kawai H, Gaffney PM, Miyauchi M, Takata T. Periostin promotes invasion and anchorage-independent growth in the metastatic process of head and neck cancer. *Cancer Res.* 2006;66:6928–6935. doi: 10.1158/0008-5472.CAN-05-4540
47. Bertero E, Canepa M, Maack C, Ameri P. Linking heart failure to cancer: background evidence and research perspectives. *Circulation.* 2018;138:735–742. doi: 10.1161/CIRCULATIONAHA.118.033603
48. Richards AM. Can heart failure cause cancer? *Nat Rev Cardiol.* 2019;16:7–8. doi: 10.1038/s41569-018-0105-x